

A Study on Microstructure and Mechanical Properties of Inconel 718 Superalloy Fabricated by Novel CMT-WAAM Process

Santhosh V^{a*} , Babu N^a

^aAlagappa Chettiar Government College of Engineering and Technology, Department of Mechanical Engineering, Karaikudi, Tamilnadu, India.

Received: May 28, 2023; Revised: November 06, 2023; Accepted: December 12, 2023

The integration of Inconel 718 (IN718) and Cold Metal Transfer (CMT) based wire + arc additive manufacturing (WAAM) for wall fabrication with a near-net shape and low buy-to-fly ratio presents a novel and promising approach with potential applications in various industrial sectors, including aerospace and automotive industries. This research aims to investigate the microstructure and mechanical anisotropy of thin-walled IN718 components that were produced using CMT based WAAM, and to compare the properties of as-deposited and heat-treated samples that underwent aerospace (AMS5663) procedures. To characterize the microstructure of the specimens, we employed optical microscopy and scanning electron microscopy (SEM) with energy dispersive spectroscopy (EDS) and an element probe microanalyzer (EPMA). Tensile and hardness tests were conducted to evaluate the mechanical properties of the specimens. Our results revealed that the as-deposited samples exhibited a dendritic microstructure with a high degree of segregation, leading to lower mechanical strength than that of the heat-treated specimens. Precipitated heat treatment promoted the precipitation of strengthening phases, such as gamma prime and carbides, improving the mechanical properties. In contrast, the precipitated heat-treated specimens exhibited a more refined microstructure with equiaxed grains and a significantly enhanced mechanical strength. This study provides critical insights into optimizing the material for different applications, leading to the development of more efficient and effective parts.

Keywords: CMT WAAM, Inconel 718, heat treatment, microstructure, mechanical properties.

1. Introduction

Inconel 718 (IN718) is a remarkable nickel based superalloy that was developed in the 1960's to meet the high-performance material demands of the aerospace and other industries¹⁻³. The alloy comprised nickel, chromium, and iron as its main components, along with small amounts of other elements like titanium, niobium, and molybdenum⁴. Its unique toughness, high strength, corrosion resistance, and oxidation resistance make it an ideal material for various applications, including gas turbine engines, rocket motors, nuclear reactors, and chemical processing equipment^{5,6}. One of the most important characteristics of IN718 is its ability to withstand high temperatures without compromising its mechanical properties. The alloy is capable of withstanding temperatures as high as 1300 °C (2372 °F), which is notably greater than the maximum operating temperature of many other alloys^{7,8}. The exceptional high-temperature capability of this alloy makes it an excellent material selection for usage in high-temperature environments of gas turbine turbines, which typically experience temperatures as high as 1100 °C (2012 °F). IN718 is known for its excellent corrosion and oxidation resistance^{9,10}. When exposed to high temperatures and harsh environments, the alloy is capable of forming a surface layer of protective oxide that inhibits further oxidation and corrosion¹¹. One of the unique features of IN 718 is its complex microstructure, which includes multiple phases such

as gamma prime (γ'), gamma (γ), and delta (δ)^{12,13}. These phases help the alloy's excellent mechanical qualities, such as its high strength, outstanding creep rupture resistance, and good fatigue resistance, to occur¹⁴. The gamma prime phase is the primary strengthening phase in IN718, making it an ideal material for high-temperature applications that require superior strength and durability. Recently, there has been increasing interest in utilizing IN718 for additive manufacturing, in particular for techniques like wire arc additive manufacturing and laser powder bed fusion^{15,16}. The aforementioned techniques possess the potential to facilitate near-net-shape fabrication, which can result in reduced material waste and increased design flexibility. Among these techniques, CMT WAAM has gained attention as a promising additive manufacturing process due to its numerous advantages over other techniques¹⁷. The CMT WAAM process is a novel manufacturing technique that employs a welding arc to liquefy a wire feedstock and deposit its layer-by-layer to fabricate the final component¹⁸. Compared to other additive manufacturing techniques like Powder Bed Fusion (PBF), Selective Laser Melting (SLM), Binder Jetting, Sheet Lamination, Laser Metal Deposition (LMD), Ultrasonic Additive Manufacturing (UAM), Plasma Spray-Based Additive Manufacturing (PSBAM) and Electron Beam Melting (EBM), CMT WAAM offers several advantages. CMT WAAM has a lower heat input, which results in less residual stress and thermal distortion in the final product.

*e-mail: santhoshshivan.v@gmail.com

In addition, CMT WAAM is a more cost-effective option and offers a higher deposition rate. This makes it an appealing method for producing components made of IN718, as it enables faster and more efficient production while reducing costs^{19,20}. The novelty of using CMT WAAM for IN718 fabrication lies in its ability to produce high-quality components with excellent mechanical properties, while being cost-effective and scalable. This process has been shown to produce parts with a high tensile strength, ductility, and fatigue resistance²¹. Moreover, the CMT WAAM process provides the capability to produce components with complex geometries on a larger scale, which can be challenging to manufacture using conventional techniques^{22,23}. Although WAAM has been applied to various metals, studies focusing on the material characteristics of IN718 fabricated using this technique are limited. Various research studies have explored the properties of IN718 produced through different AM techniques, including laser powder bed fusion (LPBF), electron beam fusion (EBM), and directed energy deposition (DED)²⁴. In a study by Xi et al.²⁵, the effect of post-treatment on the microstructure properties of LPBF-produced IN718 was investigated. The results revealed that subjecting the material to a solution heat treatment and aging process had a noteworthy effect on its ductility and toughness, while retaining its exceptional strength and hardness. Ruan et al.²⁶ used SLM to evaluate the mechanical characteristics of IN718 using a variety of process settings. Their research showed that the scanning speed used during the fabrication process had a substantial impact on the material's mechanical properties. Li et al.²⁷ investigated the welding process parameters of IN718 produced using WAAM. Reducing the travel speed and increasing the wire feed rate produced a coarser microstructure and lower tensile strength, while lowering the wire feed rate and raising the arc voltage developed a finer microstructure and greater tensile strength.

Another study by Xu²⁸ looked into the effects of preheating on WAAM-produced IN718. Their research demonstrated that preheating significantly improved the mechanical properties of the material, including tensile strength and ductility, by decreasing residual stress. Although studies of CMT based WAAM fabricated IN718 are limited, these results demonstrate that various AM techniques can produce IN718 parts with tailored microstructure characteristics and mechanical properties. This study provides important information on the microstructure and mechanical properties of IN718 fabricated using CMT WAAM combined with a robotic MIG welding system. Optical microscopy, scanning electron microscopy, energy dispersive spectroscopy (EDS), and an element probe microanalyzer (EPMA) were used to look at the intermetallic compounds and secondary carbides in the deposited and heat-treated alloys.

2. Experimental

2.1. Materials

The CMT WAAM process employs 1.2-mm-diameter Inconel 718 filler wire sourced from Special Metals. Table 1 presents the verified chemical composition of the filler wire, which adheres to ASME (American Society of Mechanical Engineers) specifications. In all cases, the substrate used for the CMT WAAM process was 15 mm thick structural S255 mild steel, which measured $300 \times 150 \times 10 \text{ mm}^{29}$.

2.2. Methods

In the CMT WAAM process experiments, a Fanuc robot (model IRB 1520ID) integrated with a Fronius TPS 400i power supply and an IRC5 controller was used, as depicted in Figure 1. Table 2 lists the process variables used for robotic inert gas metal welding.

Table 1. Chemical composition of Inconel 718 filler wire.

Elements	C	Mn	Si	S	P	Cr	Ni	Mo	Cu	Co	Nb	Ti	Al	Fe
wt-%	0.05	0.03	0.06	0.0007	0.002	17.39	52.7	2.93	0.02	0.02	5.2	0.99	0.4	20.1

Table 2. CMT WAAM process parameters.

Process Parameters	Details	Value
Deposition Power	Current	250
	Arc Voltage	26
Speed	Welding Speed / Travel speed	0.7
	Wire feed rate / speed	10
Distance and Angle	Deposit rate	1
	Layer height	4
	Contact tip to work distance	15
	Electrode to layer angle	90°
Wire	Wire grade	UNS718
	Wire Diameter	1.2
Shield gas	Shield gas type	100%
	Shield gas flow rate	15

The surface of the substrate was prepared before depositing Inconel 718 by cleaning it with a grinding wheel and removing the rust and dust with acetone. An alternating (X/Z)-raster strategy was employed, where bidirectional hatches were created in the X-direction for layer n and overlapped with the next layer $n+1$ ³⁰. A 100 mm-high layer of 74 welding passes was deposited to build the component. A detailed illustration of the deposition process and the (X/Z)-raster strategy can be seen in Figure 2. The X-axis indicates the deposition direction of each layer, while the Z-axis indicates the build direction. During printing, Cool the deposit each passes during printing to keep the interpass temperature at 300 °C to avoid overheating or warping of the components. A laser infrared thermometer gun was used to monitor the temperature of the deposits. Wire-cut EDM was used to divide the IN718 wall into two sections, followed by finishing and machining using a milling machine. Half of the wall was subjected to industrial standard heat treatments for IN718 obtained from Aerospace Material Specification (AMS5663), whereas the other half was kept as deposited. From both as-deposited and precipitate heat-treated IN718 slabs, a 10×10×10 mm³ test sample was obtained by wire-EDM cutting in the transverse (Y-Z) section. Various techniques have been utilized to prepare samples for microstructural analysis, including optical microscopy (OM), scanning electron microscopy

(SEM), energy-dispersive X-ray spectroscopy (EDX), and microhardness testing. To obtain a highly polished surface, samples were prepared for metallography using various grades of abrasive polishing paper (600–1500) and diamond pastes with particle sizes ranging from 5 to 1 μm. Subsequently, the samples were subjected to etching using a tri-mixed acid solution comprising hydrochloric, acetic, and nitric acids to expose their microstructures³¹. The microstructures of the polished and etched samples were analyzed using optical and scanning electron microscopy (SEM). Optical micrographs were acquired using a metallurgical binocular coaxial research microscope (Metzger-M Vision plus-5000 bmm software) connected to an image analyzer. A Carl Zeiss 300 Schottky Field Emission Model field-emission SEM equipped with an intelligent EDX analysis system was used to analyse and map the elements. Each Inconel-718 alloy deposit was cut in two directions to produce tensile specimens, parallel to the built-up direction and perpendicular to the deposition direction. These specimens were used to evaluate the strength of the deposited components. To measure the microhardness, the ASTM E384-11 method¹⁴ was used on the longitudinal section of the built-up orientation for both as-deposited and precipitate heat-treated IN718 alloy, with a 1 kg stress applied for 15 seconds with a MH-6 Everone Enterprises microhardness tester.

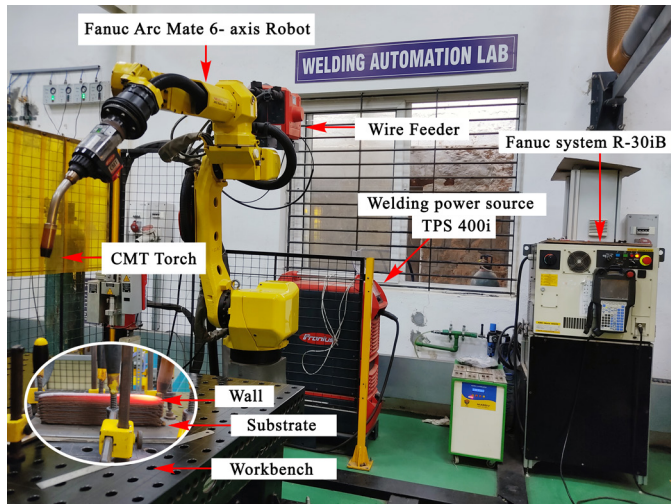


Figure 1. Cold Metal Transfer – WAAM Setup.

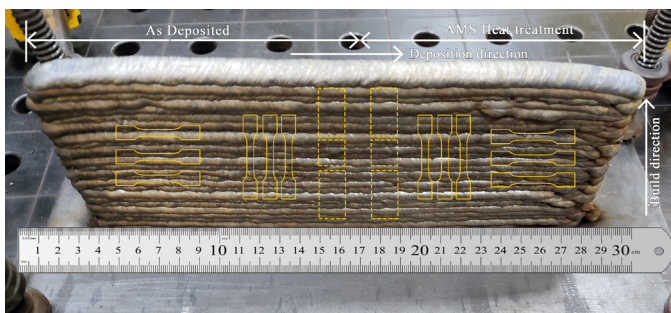


Figure 2. IN718 Fabricated wall.

2.3. Heat treatment

The CMT-WAAM process is frequently used in the aerospace industry to produce walls made of IN718, subsequently undergoing post-processing heat treatment. This process involves a solution treatment followed by low-temperature aging to create a γ'/γ'' phase. To prevent the formation of grains and improve the creep resistance, IN718 was solution-treated at lower in temperature of 980°C ³². Age hardening is another method used to achieve a desirable distribution of γ'/γ'' at lower temperatures, which leads to increase in hardness and yield strength. Age hardening involves heating the material at 718°C for 8 h, then cooling it in a furnace to 621°C for another 8 h, and keeping it at this temperature for the final 18 hours³³.

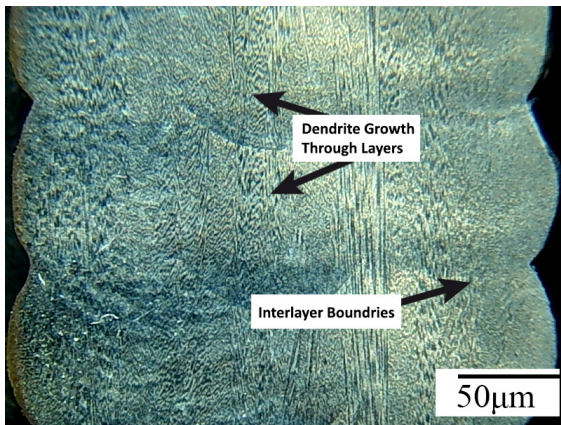


Figure 3. Macrograph – interlayer boundaries and Dendrite growth through layer.

3. Results and Discussion

3.1. Microstructure of as deposited

The metallographic specimen of IN718 exhibited a distinctive pattern of alternating light and dark bands upon etching. These bands are believed to result from the deposition of new materials and localized reheating during the building process (Figure 3). The interlayer boundaries, which showed apparent differences in dendrite patterns under light microscopy, separated the bands. The epitaxial dendrite growth, visible in the macrograph insert, suggests a significant thermal gradient in the build direction.

Interestingly, some dendrites extended across the interlayer boundaries, measuring several millimetres in length (Figure 4). Interlayer boundaries are formed owing to weak segregation banding, solute partitioning in heat-affected zones, and molten pool spreading towards the edge during deposition. Most likely, the interlayer boundary curvature results from the expansion of the molten pool during deposition. Additionally, the direction of dendrite growth at the edges of the sample showed a slight outward angle, which is a common feature observed in WAAM titanium alloys, suggesting a minor shift in the thermal gradient during metal deposition³⁴.

3.2. Laves phase, inclusions and carbides

The IN718 material was analyzed for its As-Deposited microstructure, which exhibited a range of phases, including the Laves phase and Ti- and Nb-rich inclusions present in IN718 feedstock wire. SEM images were utilized to examine the morphology and elemental composition of these particles, which provided contrast based on the topography and elemental differences³⁵. Additionally, EDX spot analysis spectra were used to identify elements in the phase particles.

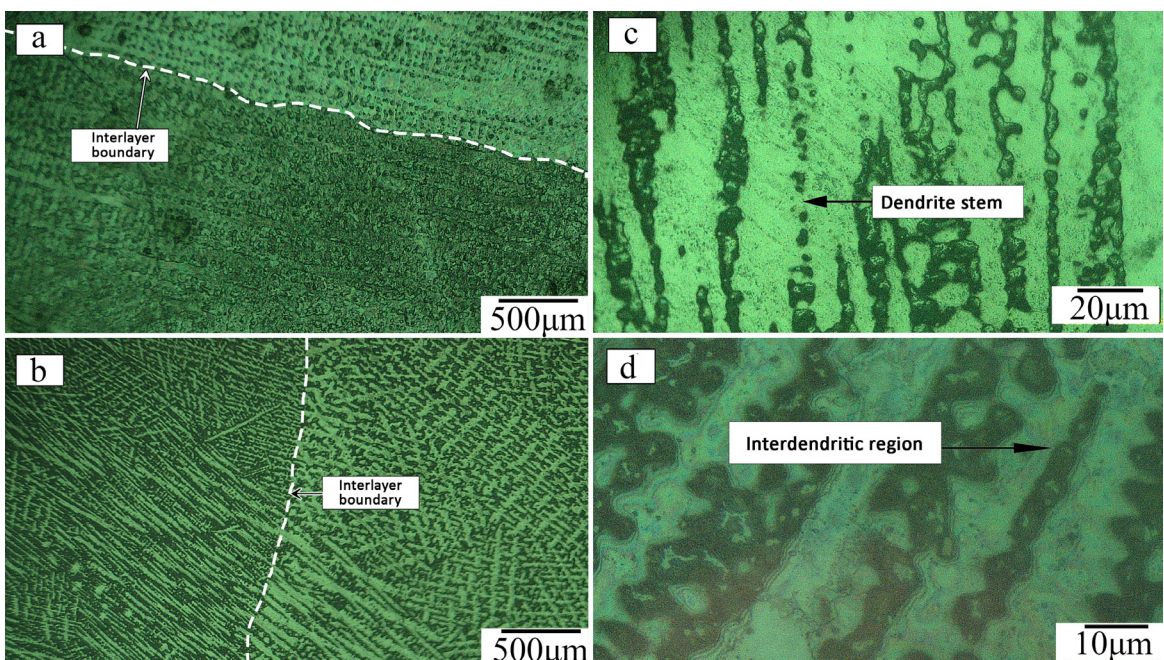


Figure 4. Optical microscope of IN718 CMT- WAAM.

As shown in Figure 5b, the corresponding spectrum shows significant peaks for dominant such substances as Ni, Cr, and Fe, which are found in the γ -matrix (Area 1 in Figure 5a) of IN718. Furthermore, the material typically exhibits smaller peaks for Nb and Mo, which is also observed in the analysis.

As-Deposited microstructure, the Laves phase displayed an island-shaped arrangement with a higher Nb and Mo concentration than the matrix because of elemental segregation, which resulted from the CMT-WAAM process's high heat input and slow cooling rate. This finding is consistent with that of a previous study on direct laser-deposited IN718. Block-shaped inclusions enriched with Ti and Nb was also

identified in the microstructure, whereas smaller peaks in the spectra were likely from the matrix. Spot 4 had a Ti-rich core and an Nb-rich shell, similar to the particles observed in IN625 fusion welds when examined using transmission electron microscopy (TEM)³⁶. Throughout the solidification of IN718, the TiN particles acted as places where carbides such as NbC could start to form. This occurred prior to the Laves phase³⁷. The TiN particles are thought to have originated from the wire feedstock. This type of Ti- and Nb-rich carbo-nitride is present in a number of IN718 materials, which suggests that the inclusions could have been caused by the thermomechanical or melting procedures used to create IN718 products.

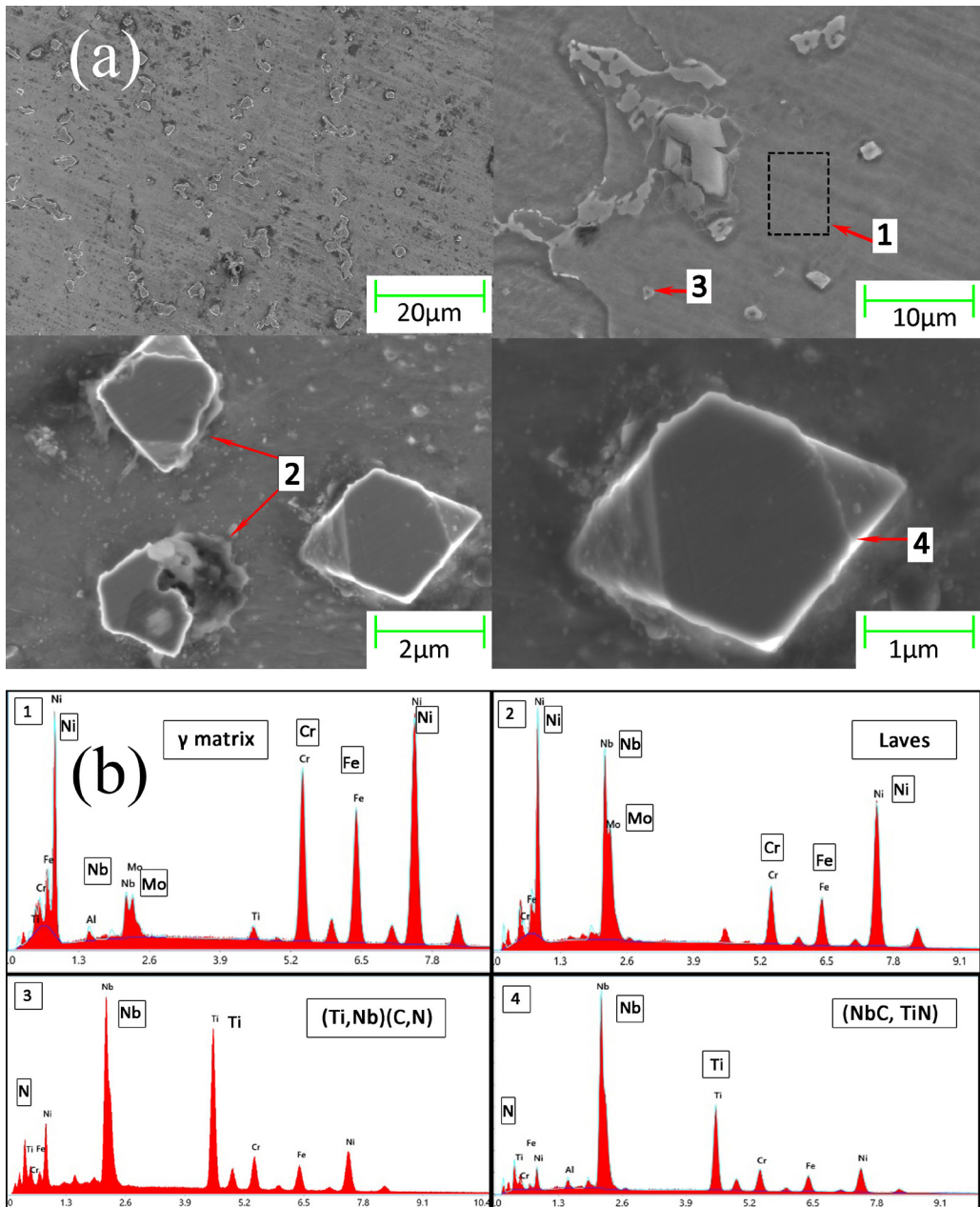


Figure 5. (a) SEM As-Deposited: SEM images of CMT WAAM IN718. (b) As-Deposited: EDS spotting of CMT WAAM IN718.

Disentangling the elements during the WAAM process causes the formation of Ti- and Nb-rich inclusions and laves phase in microstructure. This process results from a slow cooling rate and high heat input, forming a Laves phase with an island-like structure and a higher Mo and Nb content than the matrix. This observation is consistent with previous findings for direct laser-deposited IN718. Block-shaped inclusions enriched with Ti and Nb was identified using SEM images and EDX spot analysis spectra. To reduce the development of Laves phase and its effects on mechanical properties, various methods are proposed. These methods include adjusting the cooling rate, changing the chemistry of the wire feedstock, and optimizing process parameters to promote the formation of beneficial microstructures³⁸. The aim is to minimize the Laves phase on mechanical properties, such as cracking, reduced ductility, and premature failure. By addressing these problems, WAAM IN718 production will have improved mechanical properties, making it a more compelling alternative to conventional manufacturing processes.

3.3. Heat treated microstructure

Heat treatment of CMT WAAM IN718 is primarily intended to dissolve the Laves phase present in the matrix. Heat treatment proved to be effective in achieving this goal, as evident from the SEM micrograph displayed in Figure 6. The duration and temperature of the homogenization treatment are critical factors that affect the dissolution of the Laves phase, enabling the diffusion of atoms into the matrix.

In the absence of homogenization, the microstructure remained identical to As-Deposited WAAM IN718, as shown in the SEM micrograph of aging only (Figure 5a), where the Laves phase remained unchanged owing to high-temperature aging treatment. Apart from dissolving the Laves phase, the standard HSA treatment resulted in precipitation of the δ phase, which was identified by the needle-like morphology and its location at the grain boundaries (Figure 5a).

This is consistent with the results of previous studies of forged IN718 by Valle et al. Precipitation of the delta phase typically occurs between 860°C and 995°C and requires a Nb content of approximately 6-8%. In some cases, such as in laser-melted IN718, the delta phase may precipitate during solution treatment at 980 °C for 1 h, as observed in this study³⁹. The homogenization process created Nb-rich regions that influenced precipitation of δ phases in the microstructure. This was previously observed in WAAM IN718 heat-treated at 980°C for 1 h without homogenization. Several factors influence the receptivity of the microstructure to the delta phase. Titanium-rich and niobium-rich particles, such as titanium-rich nitrides and niobium-rich carbides, are minimally affected by heat treatment because their saturation solubility and eutectic temperature are greater than the treatment temperature.

3.4. Electron probe microanalysis

The EDS maps show that the distribution of solute elements in the as-deposited state and heat treatment state led to a formation of different phases. Table 3 displays the outcomes of the quantitative analysis.

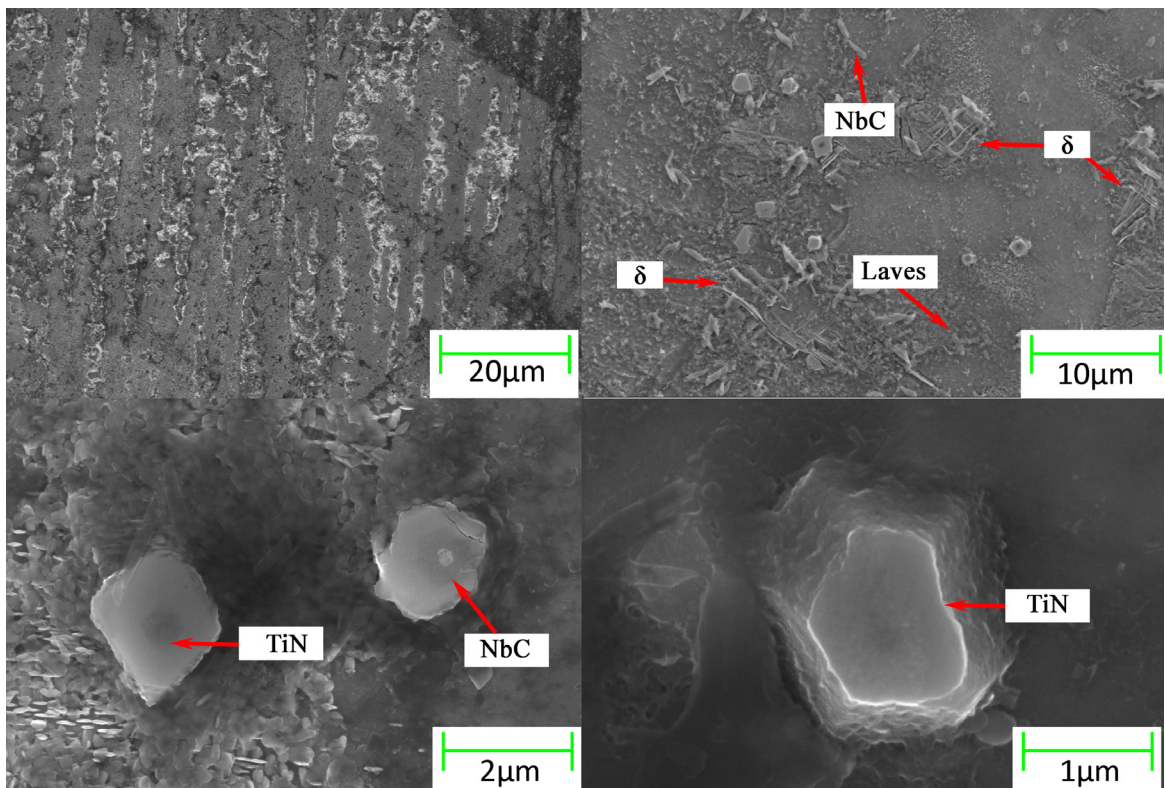


Figure 6. Heat treated: SEM images of CMT WAAM IN718.

The as-deposited state (as shown in Figure 7) showed accumulation of Ti, Mo, and Nb in the interdendritic regions, leading to the formation of TiN and NbC phases or carbonitrides and Laves phase⁴⁰. After the AMS heat treatment state (as shown in Figure 8), the redistribution of elements resulted in the development of δ Needle-shaped formations were observed in the vicinity of the partially dissolved Laves phases, and a decrease in Cr and Fe concentrations in the dendritic interphase areas due to the formation of δ phases.

4. Mechanical Properties

4.1. Hardness property

The CTM-WAAM IN718 microstructure investigation revealed non-uniformity inside each layer owing to micro segregation. This effect on the local mechanical characteristics

was investigated using the micro hardness profiles. The as-deposited samples had a sawtooth pattern with peaks around the interlayer boundaries, with a maximum of 298 HV1.0, and a minimum of 285 HV1.0. Hardness increased significantly after heat treatment owing to γ'/γ'' precipitation. Despite being in a heat-treated state, high peaks of hardness still manifested around the interlayer boundaries, with a maximum value of 454 HV1.0 and a minimum of 422 HV1.0. Figure 9 presents a comparison was made of the average hardness values between the as-deposited and heat-treated samples. The increased hardness observed in the AMS heat-treated state could be attributed to the formation of a greater number of phases following the heat treatment, Due to the high peaks of hardness observed around the interlayer boundaries, there was a limited amount of Nb available in those regions, resulting in a lower likelihood of γ'' precipitation⁴¹.

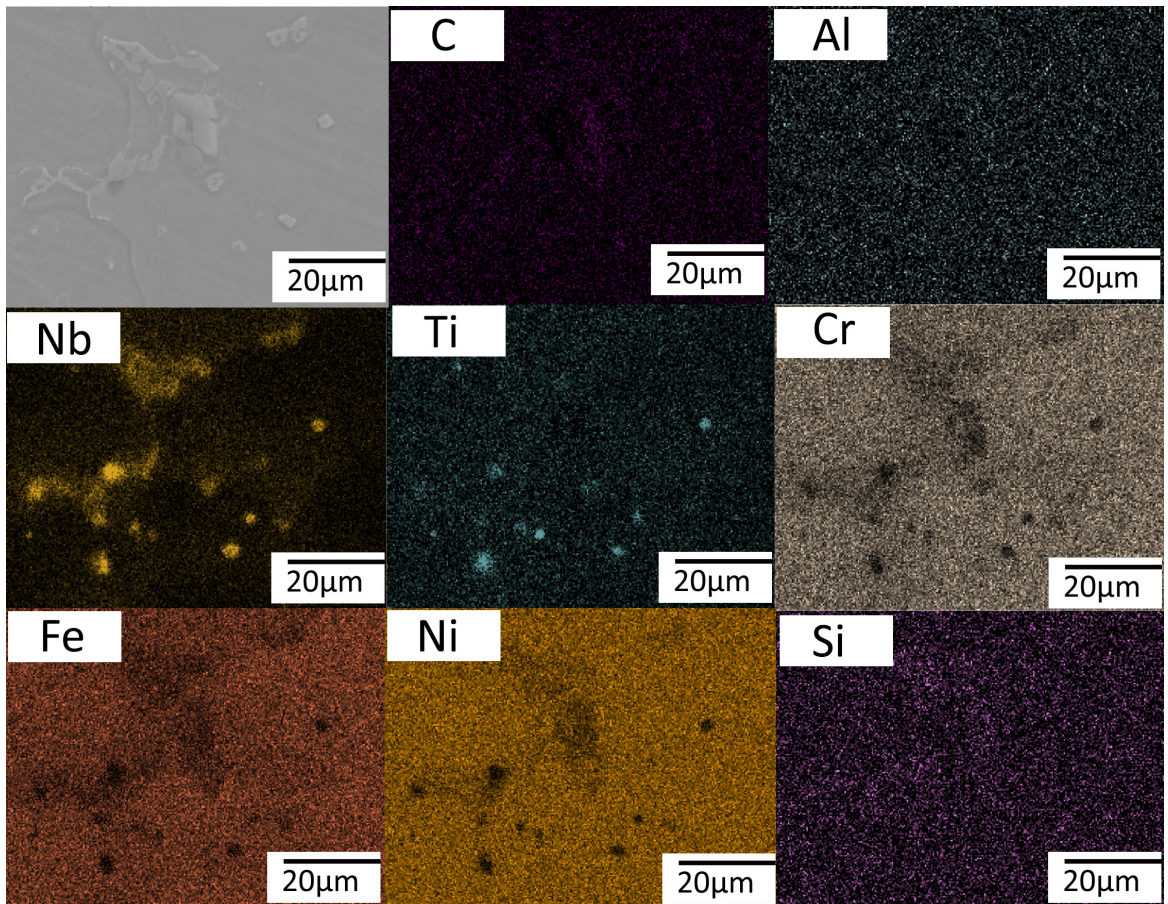


Figure 7. As- Deposited: EDS mapping of CMT WAAM IN718.

Table 3. Results of EDX- Mapping quantitative Analysis.

Description	Elements, % by weight									
	Ni	Fe	Cr	Nb	Mo	Ti	Al	C	Co	
As deposited	51.60	20.03	17.81	4.80	1.13	1.24	0.21	1.53	0.39	
Heat Treated	49.13	21.09	17.42	3.65	2.33	0.87	0.79	3.86	0.14	

4.2. Tensile Property

Figure 10 depicts the stress-strain curves used to determine the tensile properties of the material in both the build and wall axis directions in the as-deposited and heat-treated states. These characteristics are detailed in Table 4. Tensile tests were performed on CMT-WAAM IN718 in two orientations:

horizontal (H) at 90° and vertical (V) at 0° relative to the build direction. In the as-deposited state, the H specimens exhibited a higher yield strength of 498 MPa compared to the V orientation, which had the lowest yield strength because the γ'/γ'' phase was not present. The heat treatment of the specimen significantly increased the yield strength of CMT-WAAM IN718 due to the formation of the γ'/γ'' phase.

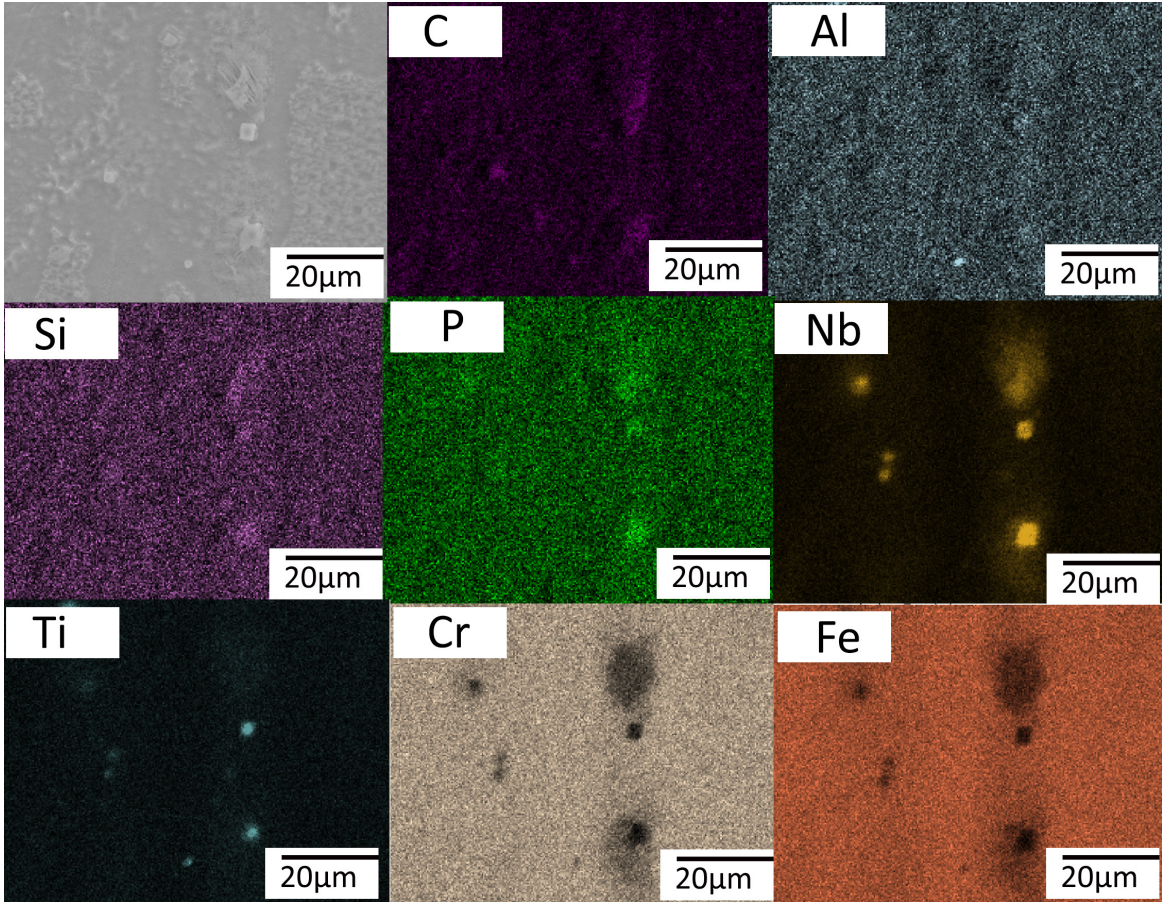


Figure 8. Heat treated: EDS mapping of CMT WAAM IN718.

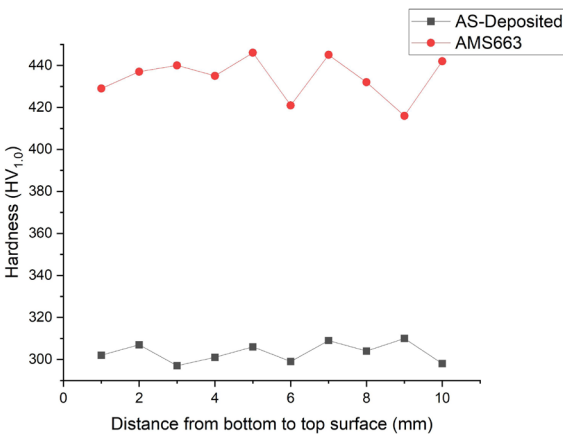


Figure 9. Micro hardness values of CMT WAAM IN718 .

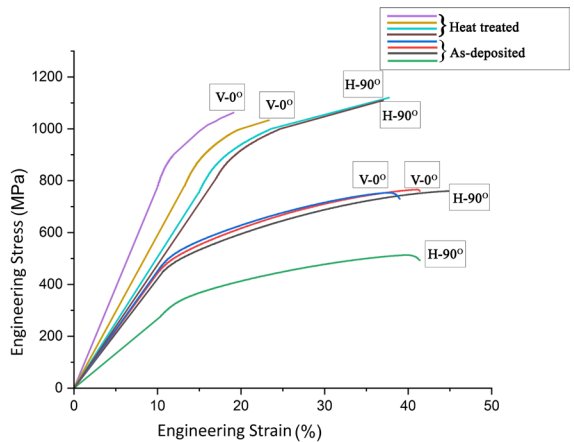


Figure 10. Stress strain curve of IN718 alloy deposit.

Table 4. Comparison of tensile strength of fabricated IN718.

Deposits		Tensile Properties		
		Ultimate tensile Strength (MPa)	Yield Strength (MPa)	Total Elongation %
As-deposited(V)0°	Sample 1	760	440	45.6
	Sample 2	766	482	41.4
As-deposited(H) 90°	Sample 1	753	498	39
	Sample 2	513	332	41.4
Heat Treated (H) 90°	Sample 1	895	790	11.8
	Sample 2	998	820	19.8
Heat Treated (V) 0°	Sample 1	1120	858	37.7
	Sample 2	1110	878	37

The specimens treated with AMS heat showed a significant improvement in yield strength in comparison to as-deposited state. The heat treatment also altered the anisotropy of the yield strength, with a higher strengthening gain in the V-orientation. Notably, the as-deposited H specimens exhibited higher yield strength compared to the V orientation due to the absence of the γ'/γ'' phase in the latter. Through a controlled heat treatment process, a significant alteration in anisotropy was achieved. The yield strength of the H orientation increased by approximately 102% (998 MPa), while the V orientation experienced an even more substantial rise of about 145% (1120 MPa). This observed shift in anisotropy underscores the role of heat treatment in tailoring directional mechanical properties of CMT-WAAM Inconel 718.

5. Conclusions

The examination of CMT-WAAM Inconel 718 yielded significant findings regarding its microstructure, mechanical characteristics, and response to heat treatment.

- i. The material's As-deposited condition featured a dendritic formation in the microstructure with Laves phases and inclusions rich in Ti and Nb, indicating micro-segregation during deposition.
- ii. Heat treatment effectively dissolves the Laves phase without causing δ precipitation, but inclusions rich in Ti and Nb remained largely unaffected. The heat-treated samples displayed higher hardness than the as-deposited ones, which can be attributed to the significant amount of precipitation of gamma prime and gamma double prime generated during the heat treatment process. This result precipitation during age hardening.
- iii. Yield strength anisotropy changed after heat treatment, with the V orientation showing a significantly higher strengthening gain than the H orientation, which displayed a 30% lower yield strength (790MPa vs 878MPa) than the as-deposited sample.

6. References

1. DebRoy T, Wei HL, Zuback JS, Mukherjee T, Elmer JW, Milewski JO, et al. Additive manufacturing of metallic components – Process, structure and properties. *Prog Mater Sci.* 2018;92:112-224. <http://dx.doi.org/10.1016/j.pmatsci.2017.10.001>.
2. Ola OT, Doern FE. A study of cold metal transfer clads in nickel-base INCONEL 718 superalloy. *Mater Des.* 2014;57:51-9. <http://dx.doi.org/10.1016/j.matdes.2013.12.060>.
3. Bandyopadhyay A, Traxel KD, Lang M, Juhasz M, Eliaz N, Bose S. Alloy design via additive manufacturing: advantages, challenges, applications and perspectives. *Mater Today.* 2022;52:207-24. <http://dx.doi.org/10.1016/j.mattod.2021.11.026>.
4. Pollock TM, Tin S. Nickel-based superalloys for advanced turbine engines: chemistry, microstructure, and properties. *J Propuls Power.* 2006;22(2):361-74. <http://dx.doi.org/10.2514/1.18239>.
5. Cacic I, Zollinger J, Engstler M, Ghanbaja J, Schenk T, El Kandaoui M, et al. Nucleation burst in additively manufactured Inconel 718: 3D characterization of ISRO-induced equiaxed microstructure. *Addit Manuf.* 2023;66:103458. <http://dx.doi.org/10.1016/j.addma.2023.103458>.
6. Xu X, Ding J, Ganguly S, Williams S. Investigation of process factors affecting mechanical properties of INCONEL 718 superalloy in wire + arc additive manufacture process. *J Mater Process Technol.* 2019;265:201-9. <http://dx.doi.org/10.1016/j.jmatprotec.2018.10.023>.
7. Zhang H, Li C, Guo Q, Ma Z, Huang Y, Li H, et al. Hot tensile behavior of cold-rolled Inconel 718 alloy at 650 °C: the role of δ phase. *Mater Sci Eng A.* 2018;722:136-46. <http://dx.doi.org/10.1016/j.msea.2018.02.093>.
8. Lan B, Wang Y, Liu Y, Hooper P, Hopper C, Zhang G, et al. The influence of microstructural anisotropy on the hot deformation of wire arc additive manufactured (WAAM) Inconel 718. *Mater Sci Eng A.* 2021;823:141733. <http://dx.doi.org/10.1016/j.msea.2021.141733>.
9. Kang YJ, Yang S, Kim YK, AlMangour B, Lee K-A. Effect of post-treatment on the microstructure and high-temperature oxidation behaviour of additively manufactured Inconel 718 alloy. *Corros Sci.* 2019;158:108082. <http://dx.doi.org/10.1016/j.corsci.2019.06.030>.
10. Sanviemvongsak T, Monceau D, Desgranges C, Macquaire B. Intergranular oxidation of Ni-base alloy 718 with a focus on additive manufacturing. *Corros Sci.* 2020;170:108684. <http://dx.doi.org/10.1016/j.corsci.2020.108684>.
11. Sanviemvongsak T, Monceau D, Macquaire B. High temperature oxidation of IN 718 manufactured by laser beam melting and electron beam melting: effect of surface topography. *Corros Sci.* 2018;141:127-45. <http://dx.doi.org/10.1016/j.corsci.2018.07.005>.
12. Zhou L, Mehta A, McWilliams B, Cho K, Sohn Y. Microstructure, precipitates and mechanical properties of powder bed fused inconel 718 before and after heat treatment. *J Mater Sci Technol.* 2019;35(6):1153-64. <http://dx.doi.org/10.1016/j.jmst.2018.12.006>.
13. Wang K, Liu Y, Sun Z, Lin J, Lv Y, Xu B. Microstructural evolution and mechanical properties of Inconel 718 superalloy thin wall fabricated by pulsed plasma arc additive manufacturing. *J Alloys Compd.* 2020;819:152936. <http://dx.doi.org/10.1016/j.jallcom.2019.152936>.
14. Chen Z, Soh GS. Microstructure and mechanical properties of Wire Arc Additive Manufactured (WAAM) Inconel 718 parts via post heat treatments. *Mater Today Proc.* 2022;70:567-73. <http://dx.doi.org/10.1016/j.matpr.2022.09.592>.

15. Li Z, Chen J, Sui S, Zhong C, Lu X, Lin X. The microstructure evolution and tensile properties of Inconel 718 fabricated by high-deposition-rate laser directed energy deposition. *Addit Manuf.* 2020;31:100941. <http://dx.doi.org/10.1016/j.addma.2019.100941>.
16. Ju J, Yang T. (2023) Microstructural understanding of high-temperature oxidation behaviour of selective laser melted Inconel 718 superalloy in Co2 atmosphere. *SSRN Electron J.* 1-29. <https://doi.org/10.2139/SSRN.4365838>.
17. Ola OT, Doern FE. A study of cold metal transfer clads in nickel-base INCONEL 718 superalloy. *Mater Des.* 2014;57:51-9. <http://dx.doi.org/10.1016/j.matdes.2013.12.060>.
18. Kindermann RM, Roy MJ, Morana R, Prangnell PB. Process response of Inconel 718 to wire + arc additive manufacturing with cold metal transfer. *Mater Des.* 2020;195:109031. <http://dx.doi.org/10.1016/j.matdes.2020.109031>.
19. Jackson MA, Van Asten A, Morrow JD, Min S, Pfefferkorn FE. A comparison of energy consumption in wire-based and powder-based additive-subtractive manufacturing. *Procedia Manuf.* 2016;5:989-1005. <http://dx.doi.org/10.1016/j.promfg.2016.08.087>.
20. Lu X, Li MV, Yang H. Comparison of wire-arc and powder-laser additive manufacturing for IN718 superalloy: unified consideration for selecting process parameters based on volumetric energy density. *Int J Adv Manuf Technol.* 2021;114(5-6):1517-31. <http://dx.doi.org/10.1007/s00170-021-06990-y>.
21. Hosseini E, Popovich VA. A review of mechanical properties of additively manufactured Inconel 718. *Addit Manuf.* 2019;30:100877. <http://dx.doi.org/10.1016/j.addma.2019.100877>.
22. Jia T, Zou B, Liu W, Lei T, Ding H. Effect of process parameters on mechanical properties of Inconel718 superalloy fabricated by directional energy deposition. *Int J Adv Manuf Technol.* 2023;128(7-8):2863-83. <http://dx.doi.org/10.1007/s00170-023-10854-y>.
23. Range M, Temperature C. *Special Metals Inconel G-3. Alloy Dig.* 2021;70(8):Ni-774. <http://dx.doi.org/10.31399/asm.ad.ni0774>.
24. Moreira MF, Fantin LB, Beneduce Neto F, Azevedo CRF. Microstructural and mechanical characterization of as-cast nickel-based superalloy (IN-713C). *Int J Met Cast.* 2021;15(4):1129-48. <http://dx.doi.org/10.1007/s40962-020-00540-0>.
25. Xi N, Tang K, Fang X, Li Y, Duan Y, Huang K. Enhanced comprehensive properties of directed energy deposited Inconel 718 by a novel integrated deposition strategy. *J Mater Sci Technol.* 2023;141:42-55. <http://dx.doi.org/10.1016/j.jmst.2022.09.026>.
26. Ruan G, Liu C, Qu H, Guo C, Li G, Li X, et al. A comparative study on laser powder bed fusion of IN718 powders produced by gas atomization and plasma rotating electrode process. *Mater Sci Eng A.* 2022;850:143589. <http://dx.doi.org/10.1016/j.msea.2022.143589>.
27. Li Y, Založnik M, Zollinger J, Dembinski L, Mathieu A. Effects of the powder, laser parameters and surface conditions on the molten pool formation in the selective laser melting of IN718. *J Mater Process Technol.* 2021;289:116930. <http://dx.doi.org/10.1016/j.jmatprotec.2020.116930>.
28. Xu W. Direct additive manufacturing techniques for metal parts: SLM, EBM, Laser Metal Deposition. *Encycl Mater Met Alloy.* 2022;3:290-318. <https://doi.org/10.1016/B978-0-12-819726-4.00095-8>.
29. Bai P, Huo P, Wang J, Yang C, Zhao Z, Zhang Z, et al. Microstructural evolution and mechanical properties of Inconel 718 alloy manufactured by selective laser melting after solution and double aging treatments. *J Alloys Compd.* 2022;911:164988. <http://dx.doi.org/10.1016/j.jallcom.2022.164988>.
30. Yu X, Lin X, Liu F, Wang L, Tang Y, Li J, et al. Influence of post-heat-treatment on the microstructure and fracture toughness properties of Inconel 718 fabricated with laser directed energy deposition additive manufacturing. *Mater Sci Eng A.* 2020;798:140092. <http://dx.doi.org/10.1016/j.msea.2020.140092>.
31. Seow CE, Coules HE, Wu G, Khan RHU, Xu X, Williams S. Wire + arc additively manufactured Inconel 718: effect of post-deposition heat treatments on microstructure and tensile properties. *Mater Des.* 2019;183:1-13. <http://dx.doi.org/10.1016/j.matdes.2019.108157>.
32. Sohrabi MJ, Mirzadeh H, Rafei M. Solidification behavior and Laves phase dissolution during homogenization heat treatment of Inconel 718 superalloy. *Vacuum.* 2018;154:235-43. <http://dx.doi.org/10.1016/j.vacuum.2018.05.019>.
33. Ho A, Zhao H, Fellowes JW, Martina F, Davis AE, Prangnell PB. On the origin of microstructural banding in Ti-6Al4V wire-arc based high deposition rate additive manufacturing. *Acta Mater.* 2019;166:306-23. <http://dx.doi.org/10.1016/j.actamat.2018.12.038>.
34. Sujan GK, Li H, Pan Z, Liang D, Alam N. Microstructural characterization and oxidation performance of solution-annealed and precipitation hardened wire-arc additively manufactured Inconel 718 superalloys. *Addit Manuf.* 2022;51:102602. <http://dx.doi.org/10.1016/j.addma.2022.102602>.
35. Silva CC, Miranda HC, Motta MF, Farias JP, Afonso CRM, Ramirez AJ. New insight on the solidification path of an alloy 625 weld overlay. *J Mater Res Technol.* 2013;2(3):228-37. <http://dx.doi.org/10.1016/j.jmrt.2013.02.008>.
36. Cockcroft SL, Degawa T, Mitchell A, Tripp DW, Schmalz A. Inclusion precipitation in superalloys. 2012;577-86. http://dx.doi.org/10.7449/1992/Superalloys_1992_577_586.
37. Jia Z, Wan X, Guo D. Study on microstructure and mechanical properties of Inconel718 components fabricated by UHFP-GTAW technology. *Mater Lett.* 2020;261:127006. <http://dx.doi.org/10.1016/j.matlet.2019.127006>.
38. Liu Q, Chen C, Zhang M, Wang S. Effect of different heat treatments on the microstructural evolution and mechanical properties of Ni-Cr-Si alloy fabricated by laser additive manufacturing. *J Mater Eng Perform.* 2019;28(8):4543-55. <http://dx.doi.org/10.1007/s11665-019-04239-0>.
39. Radhakrishna C, Prasad Rao K. The formation and control of Laves phase in superalloy 718 welds. *J Mater Sci.* 1997;32:1977-84. <https://doi.org/10.1023/A:1018541915113>.
40. Ferreri NC, Vogel SC, Knezevic M. Determining volume fractions of γ , γ' , γ'' , δ , and MC-carbide phases in Inconel 718 as a function of its processing history using an advanced neutron diffraction procedure. *Mater Sci Eng A.* 2020;781:139228. <http://dx.doi.org/10.1016/j.msea.2020.139228>.
41. Xu X, Ding J, Ganguly S, Williams S. Investigation of process factors affecting mechanical properties of INCONEL 718 superalloy in wire + arc additive manufacture process. *J Mater Process Technol.* 2019;265:201-9. <http://dx.doi.org/10.1016/j.jmatprotec.2018.10.023>.